Journal of Fluids and Structures (1998) **12,** 511–536
Article No.: fl980161

GUST LOADING ON STREAMLINED BRIDGE DECKS

G. L. Larose

Department of Structural Engineering and Materials, Technical University of Denmark 2800 Lyngby, Denmark†

AND

J. Mann

Risoe National Laboratory, 4000 Roskilde, Denmark

(Received 28 July 1997 and in revised form 3 February 1998)

The current analytical description of the buffeting action of wind on long-span bridges is based on the strip assumption. However, recent experiments on closed-box girder bridge decks have shown that this assumption is not valid and is the source of an important part of the error margin of the analytical prediction methods. In this paper, an analytical model that departs from the strip assumption is used to describe the gust loading on a thin airfoil. A parallel is drawn between the analytical model and direct measurements of gust loading on motionless closed-box girder bridge decks. Empirical models of aerodynamic admittance and span-wise coherence of the aerodynamic forces are proposed for a family of deck cross-sections.

1. INTRODUCTION

In the theory of buffeting of slender line-like structures, Davenport (1962) clearly stated the assumptions made as well as the limitations of the theory. One assumption concerns the size of the structure in relation to the size of the gusts:
"*... that the structures* (*or structural members*) *are sufficiently slender for the secondary span-wise flow and redistribution of pressures to be neglected, such that the pressures on any section of the span are only due to the wind incident on that section*; ...".

This referred to the strip assumption which was also used by Liepmann (1952) as a solution to the buffeting problem of aircraft wings. Davenport (1962) commented that this assumption seemed reasonable for a thin cable or an open-lattice truss but was not likely to be valid for structures with larger aspect ratios such as buildings.

Experience has shown that this assumption appeared to be valid for the case of buffeting drag forces on slender structures where the characteristic length of the body could be more than 100 times smaller than the scales of the longitudinal components of the turbulence (Vickery, 1966). However, for the buffeting lift forces, where the characteristic length of the structure can be the width of a closed-box girder bridge deck, $\approx$20–35 m, and the length scales of the vertical gusts could be of the order of $\approx$30–50 m, the assumption failed, as originally expected by Davenport.

†Now at the Danish Maritime Institute, Hjortekærsvej 99, 2800 Lyngby, Denmark

0889–9746/98/050511 + 26 $30.00

The non-validity of the strip assumption for the lift and overturning moment buffeting analysis has been shown experimentally on many occasions, first by Nettleton on an airfoil in grid turbulence, in Ektin (1971), then by Melbourne (1982) in full scale and model scale on the West Gate Bridge and more recently by Larose (1992), Larose *et al.* (1993), Sankaran & Jancauskas (1993), Kimura *et al.* (1996), and Bogunovic Jakobsen (1995). Larose (1997) evaluated the error margin of the variance of the buffeting response associated with the use of the strip assumption. For lift, it varied between a 70% underestimation for a reduced velocity of 2 to a 100% overestimation for a reduced velocity of 20.

The strip assumption is, nevertheless, the basis of the current buffeting theory of line-like structures, both for the frequency-domain and time-domain approaches. The objective of this paper is to propose the use of a model of the buffeting wind loads on streamlined bridge decks that departs from the strip assumption and reduces the error margin of the analytical prediction methods. The appellation "streamlined" refers to closed-box girder bridge decks that have been designed with emphasis put on aerodynamics but are strictly speaking bluff bodies with separated shear layers.

2. THEORY: LIFT FORCE INDUCED BY TURBULENCE

In this section the simplest analytical model of the lift forces induced by the gustiness of the wind acting on a motionless bridge deck is discussed. Only the vertical gusts (w component of the wind fluctuations) are considered and it is assumed that the deck cross-section is slender enough to have aerodynamic characteristics similar to a thin airfoil (flat plate).

The two main assumptions that were put forward to bring an approximate solution to the problem are: (i) quasi-steady aerodynamics and (ii) the strip assumption. The quasi-steady assumption implies that the lift force at a position y at the time t on a bridge deck is equal to the force that would have existed if the instantaneous velocity $w(t, y)$ persisted for an infinitely long time everywhere on the deck.

Under the strip assumption, the lift force (per unit length) on a strip at a position y along the bridge deck is equal to the lift force per unit length that would have been if the wind fluctuations had been fully correlated along the deck. The forces on a strip are thus assumed to be induced by the gust acting on that strip only, without considering the gusts on the neighbouring strips.

For an airfoil, the applicability of Sears' analysis of the unsteady lift forces induced by a transversely fully coherent sinusoidal gust [in Fung (1969)] is based on the strip assumption.

2.1. Quasi-Steady Aerodynamics

For a flat plate with a lift slope C_z' of 2π, the quasi-steady assumption implies

$$F_z(x, y) = 2\pi w(x, y), \tag{1}$$

where the lift F_z has been normalized suitably, and instead of t the coordinate in the flow direction, $x = -\bar{V}t$ is used ($\bar{V}$ is the mean wind speed, see Figure 1). The covariance function of the lift force is defined, assuming $\langle F_z \rangle = 0$, as

$$R_L(x, y) = \langle F_z(x', y') F_z(x' + x, y' + y) \rangle, \tag{2}$$

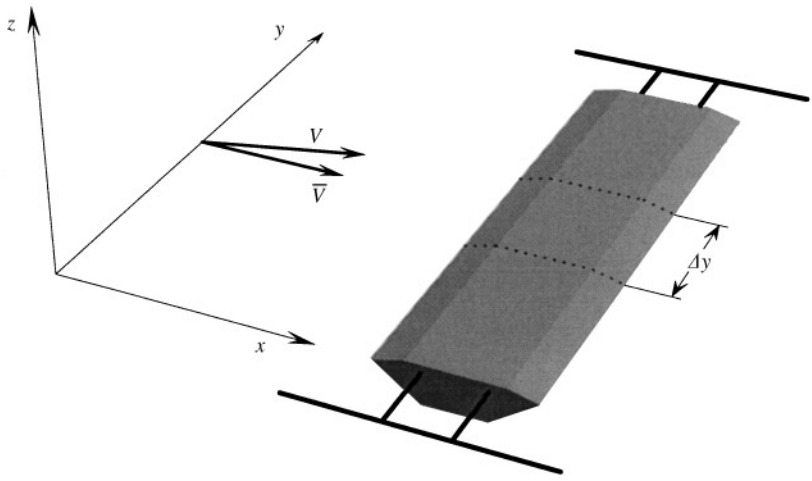

Figure 1. The coordinate system has the x-axis in the direction of the mean wind $\bar{V}$, y along the bridge deck, and z perpendicular to the two other axes. V is an instantaneous wind velocity deviating randomly from $\bar{V}$ and Δy is the separation between strips equipped with pressure transducers.

where $\langle\ \rangle$ denotes ensemble averaging. The one- and two-dimensional spectra of the lift force are defined as

$$S_L(k_1) = \frac{1}{2\pi}\int_{-\infty}^{\infty} R_L(x, 0)\exp(-\mathrm{i}k_1 x)\,\mathrm{d}x \tag{3}$$

and

$$S_L(k_1, k_2) = \frac{1}{(2\pi)^2}\int_{-\infty}^{\infty}\int_{-\infty}^{\infty} R_L(x, y)\exp[-\mathrm{i}(k_1 x + k_2 y)]\,\mathrm{d}x\,\mathrm{d}y, \tag{4}$$

and similarly for the vertical wind speed w.

Fourier transforming the covariance function of both sides of equation (1) in the x- and y-direction, the two-dimensional lift force spectrum is obtained:

$$S_L(k_1, k_2) = 4\pi^2 S_w(k_1, k_2). \tag{5}$$

Equation (5) can be reduced to a one-dimensional force spectrum by

$$S_L(k_1) = \int_{-\infty}^{\infty} S_L(k_1, k_2)\,\mathrm{d}k_2 \tag{6}$$

$$= 4\pi^2 S_w(k_1). \tag{7}$$

The cross-spectrum of the lift forces between strips at points 1 and 2 separated by Δy, $S_{L_1L_2}(k_1, \Delta y)$‡ can also be derived from the two-dimensional spectrum:

$$S_{L_1L_2}(k_1, \Delta y) = \int_{-\infty}^{\infty} S_L(k_1, k_2)\mathrm{e}^{\mathrm{i}k_2\Delta y}\,\mathrm{d}k_2. \tag{8}$$

‡Note that the symbols S_L has several different meanings: $S_L(k_1)$ is the force spectrum measured on one strip of the infinitely long airfoil, $S_{L_1L_2}(k_1, \Delta y)$ is the cross-spectrum calculated from measurement at two strips separated by Δy, and $S_L(k_1, k_2)$ is the two-dimensional force spectrum. This could, in principle, be evaluated by measuring forces at any point along the foil and in time, and Fourier transforming both in t and y.

The span-wise root coherence of the lift forces, $\mathrm{coh}_L^{1/2}$, is obtained by dividing the cross-spectrum by the one-dimensional force spectrum:

$$\mathrm{coh}_L^{1/2}(k_1, \Delta y) \equiv \frac{S_{L_1 L_2}(k_1, \Delta y)}{S_L(k_1)}. \tag{9}$$

2.2. Introducing Unsteadiness

Faced with the problem of the unsteady nature of the lift forces due to wind gusts, Sears investigated the forces on an airfoil due to a special vertical velocity spectrum [in Fung (1969)]:

$$S_w(k_1, k_2) = S_w(k_1)\delta(k_2), \tag{10}$$

where δ is Dirac's delta function; that is, gusts with sinusoidal variations of w only in the direction of the mean flow (x) and no variations in the y direction, or fully correlated gusts.

Sears found from the linearized equations of fluid motion and the Kutta–Joukowski condition (no singularities at the rear end of the airfoil) that

$$S_L(k_1) = 4\pi^2 |\phi(\tilde{k}_1)|^2 S_w(k_1), \tag{11}$$

where $\tilde{k}_1 = k_1 B/2$, B is the deck width (or the chord of the airfoil), and

$$|\phi(\tilde{k}_1)|^2 = \left| \frac{\mathrm{J}_0(\tilde{k}_1)\mathrm{K}_1(i\tilde{k}_1) + \mathrm{i}\mathrm{J}_1(\tilde{k}_1)\mathrm{K}_0(i\tilde{k}_1)}{\mathrm{K}_1(i\tilde{k}_1) + \mathrm{K}_0(i\tilde{k}_1)} \right|^2 \quad \text{(Sears' function)}. \tag{12}$$

$\mathrm{J}_0, \mathrm{J}_1$ are Bessel functions and $\mathrm{K}_0, \mathrm{K}_1$ are modified Bessel functions of the second kind.

An approximation to Sears' function was proposed by Liepmann and is of the form

$$|\phi(\tilde{k}_1)|^2 \approx \frac{1}{1 + 2\pi\tilde{k}_1} \quad \text{(Liepmann's approximation)}. \tag{13}$$

With equations (11) and (13), it is clear that the lift forces are reduced as k_1 increases. The unsteady forces are also smaller than one would expect if quasi-steady conditions were applicable. Sears demonstrated that for any variation of the wavenumber above 0 (i.e. for any flow fluctuation with a finite wavelength) the fluctuating lift will be less than the quasi-steady value.

This reduction of lift with wavenumber is generally represented by the aerodynamic admittance. It can be seen as a measure of the effectiveness of a body in extracting energy from the various frequency components of the turbulence.

The aerodynamic admittance can be defined as

$$A(k_1) = \frac{S_L(k_1)}{C_z'^2 S_w(k_1)}. \tag{14}$$

Based on this definition and on equation (7) $A(k_1) = 1.0$ for the quasi-steady case. For a thin airfoil in a fully correlated gust (which is equivalent to the strip assumption),

$$A(k_1) = |\phi(\tilde{k}_1)|^2. \tag{15}$$

Applying the strip assumption it is also possible to calculate the span-wise root coherence of the forces,

$$\mathrm{coh}_L^{1/2}(k_1, \Delta y) = \mathrm{coh}_w^{1/2}(k_1, \Delta y). \tag{16}$$

Sears' function (or Liepmann's approximation to Sears' function) is often used in bridge aerodynamics to represent the aerodynamic admittance. It tends to 1.0 for $f \to 0$. Experiments in turbulent flow on section models of streamlined bridge decks have shown that the admittance tends to be lower than equation (12) for low frequencies and, if the bridge deck is bluff, higher at high frequencies (Larose 1992). Furthermore, the span-wise root coherence of the lift forces was found to be much higher than for w in clear contrast to equation (16) (Larose *et al.* 1993; Kimura *et al.* 1996; Bogunovic Jacobsen 1995).

2.3. Lifting the Strip Assumption

The natural extension to Sears' analysis is due to Graham (1970) from an original suggestion by Ribner [in Jackson *et al.* (1973)]. Ribner proposed in 1957, as an alternative approach to the strip assumption method, to calculate the unsteady lift for an incident flow field represented by a superposition of plane sinusoidal wave motions of all orientations and wavelengths [equivalent to $S_w(k_1, k_2)$]. This required a two-wavenumber aerodynamic admittance.

Graham (1970) numerically computed the exact two-wavenumber aerodynamic admittance using lifting-surface theory for an airfoil of infinite span length due to gusts with arbitrary horizontal wavevectors (k_1, k_2). In his derivation, Graham used the same linear assumption as in Sears' analysis but worked with yawed sinusoidal gusts that could vary in y as well as in x. That is to say that a chord-wise strip could be partially immersed in a gust oncoming from a certain horizontal direction but also be influenced by a gust from a different direction. This is departing from the strip assumption and it is a better representation of the physics of incident gusts being distorted and diverted as they approach the body. An experimental validation of Graham's approach is presented by Jackson *et al.* (1973).

The two-wavenumber spectrum of the lift forces becomes

$$S_L(k_1, k_2) = 4\pi^2 |\phi(\tilde{k}_1, \tilde{k}_2)|^2 S_w(k_1, k_2), \tag{17}$$

where

$$|\phi(\tilde{k}, \tilde{k}_2)|^2 \approx \frac{1}{1 + 2\pi\tilde{k}_1}\left[\frac{\tilde{k}_1^2 + 2/\pi^2}{\tilde{k}_1^2 + \tilde{k}_2^2 + 2/\pi^2}\right]. \tag{18}$$

Equation (18) is an approximate closed-form expression due to Mugridge (1971) of the aerodynamic admittance. It is presented as a correction factor to the Sears ' function. It reduces to equation (13) for fully coherent gusts (when $\tilde{k}_2 = 0$).

Other approximate closed-form expressions of Graham's exact solution exist, namely by Filotas, in Mugridge (1971), and by Blake (1986); however, Mugridge's approximation is most valid for the lower wavenumber range ($k_1 < 2$) which is the range of interest for bridge aerodynamics.

2.3.1. *Application of the two-wavenumber model*

Using equation (17) it can be shown that $A(k_1)$ does not tend to 1.0 as $k_1 \to 0$ (Jackson *et al.* 1973). This is in agreement, at least qualitatively, with results of experiments on thin airfoils and bridge decks.

The span-wise coherence is linked to the cross-sectional admittance through equations (8) and (9). Mann (1995) has calculated the cross-spectrum and the span-wise coherence of the lift forces on a thin airfoil in isotropic turbulence based on equations (8), (17) and Mugridge's approximation (18). It resulted in $\mathrm{coh}_L^{1/2} > \mathrm{coh}_w^{1/2}$, confirming several experimental observations of the non-validity of the strip assumption. Section 3.2 presents similar calculations.

3. EXPERIMENTAL VALIDATION

All the quantities of Section 2.3 can be measured directly or evaluated indirectly in controlled experiments on section models in a wind tunnel. The validation of the two-wavenumber model (referred to later as the 3-D model) of the lift force is thus possible.

The ideal case would have been to conduct a series of experiments in isotropic turbulence on a thin airfoil with a lift slope approaching 2π. However, the ultimate objective of this research being the application of the 3-D model to bridge aerodynamics, the experiments were conducted on section models with cross-sectional dimensions and proportions typical of modern closed-box girder bridge decks.

3.1. The Experiments

Direct measurements of the buffeting forces on motionless section models in turbulent flow were conducted in Boundary Layer Wind Tunnel-II of the Danish Maritime Institute (DMI). The dynamic force measurements were based on simultaneous measurements of unsteady surface pressures on three chord-wise strips of the section models, the span-wise separations of the strips being adjustable. The cross-sections studied were typical closed-box girder bridge decks as seen in Figure 2.

The parameters of the experiments were: the width-to-depth ratio B/D of the section models, the length scale of turbulence, the presence or lack of railings and the influence of the angle of the angle of wind incidence. A detailed account of the experiments is given in Larose (1997).

For each case, power spectral densities of the lift and torque coefficients were calculated as well as the span-wise coherence of the buffeting forces.

3.1.1. *Description of the incident turbulent flow field*

Three turbulent wind fields were used in the parametric investigations of the buffeting forces, two generated by spires placed 15 m upstream of the model and one by a coarse grid placed 4.6 m upstream. The two spire sets gave similar length scales of turbulence but different turbulence intensities, while the position of the grid was selected to match the turbulence intensity of one of the spire sets but giving much smaller length scales. The spires also gave a slight anisotropy to the flow.

The grid had an isotropic mesh of 0.34 m with a bar size of 0.085 m. The medium spires, in a set of three, were 0.32 m wide at the base, 0.20 m at the top and 1.8 m high, while the large

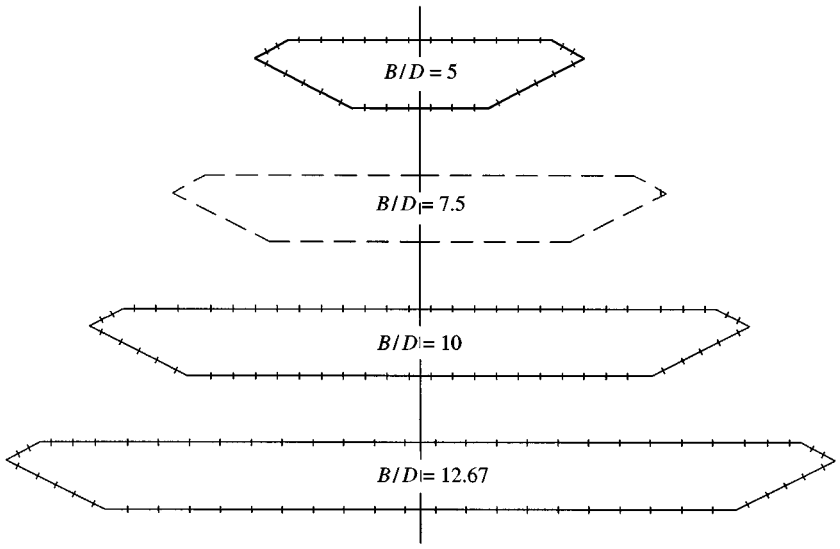

Figure 2. Cross-sectional shape of the models investigated. The $B/D = 7.5$ cross-section was studied on another occasion and the results are reported in Larose (1992).

spires were 0.36 m at the base, 0.23 m at the top and 1.72 m high. The tests in the wind tunnel were typically conducted at a mean wind speed of 15 m s^{-1}.

For each wind field, the u, v and w components of the wind were fitted with the isotropic turbulence model based on the von Kármán spectrum described by Mann (1994). The spectral tensor fitted particularly well the span-wise root coherence (or co-coherence) measurements made by hot-wire anemometry.

The one-point spectrum of the w-component was fitted with

$$S_w(k_1) = \frac{3}{110}\,\alpha\varepsilon^{2/3}\,\frac{3L^{-2} + 8k_1^2}{(L^{-2} + k_1^2)^{11/6}}, \tag{19}$$

where L is a length scale and $\alpha\varepsilon^{2/3}$ represents the rate of dissipation of turbulent kinetic energy. Both quantities were obtained by a least-squares fit of the measured spectra. L was converted to $\mathscr{L}$, the wavelength associated with the peak of the spectrum in its $k_1 S_w(k_1)$ representation, using

$$\mathscr{L}_w = \frac{2}{(6 + 3\sqrt{5})^{1/2}}\,L \approx 0.561L. \tag{20}$$

$\mathscr{L}$ was preferred to the conventional integral length scale since it represents the wavelength of the gusts that carry most of the energy of the turbulence. Examples of fits using equation (19) are shown in Figure 3. The resulting ratios between the length scales and the deck widths studied, $\mathscr{L}_w/B$, are given in Table 1.

3.1.2. *Measured aerodynamic admittance functions*

The aerodynamic admittances were calculated based on the experimental determination of the spectrum of the lift coefficient $S_{C_z}(f)$, the lift slope and the spectra of the u and

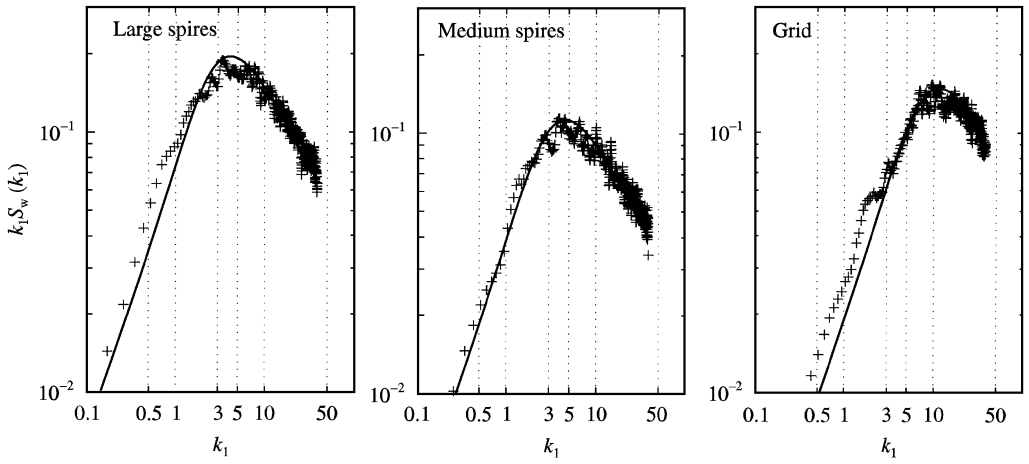

Figure 3. Spectra of the vertical wind fluctuations for the three cases of this study. Solid line: fit of von Kármán spectrum using equation (19).

TABLE 1
Characteristics of flow conditions for the three wind field cases in relation to the width of the models based on the least-squares fit of the von Kármán spectrum

Cases	w-component				$\mathscr{L}_w/B$		
	I_w (%)	L (m)	$\alpha\varepsilon^{2/3}$ ($m^{4/3}/s^2$)	$\mathscr{L}_w$ (m)	$B/D = 5$	$B/D = 10$	$B/D = 12.67$
Large spires	8.8	0.43	3.4	0.24	–	0.80	0.63
Medium spires	7.2	0.39	2.1	0.22	1.50	0.73	0.58
Grid	7.6	0.15	5.1	0.09	0.57	0.29	0.23

w component of the oncoming wind fluctuations. The following expression was used:

$$|A_z(f)|^2 = \frac{\bar{V}^2 S_{C_z}(f)}{4C_z^2 S_u(f) + C_z'^2 S_w(f)}. \tag{21}$$

The contribution of the u-component can be considered negligible for the cross-sections studied here, as can be evaluated based on the static coefficients of Table 2.

Results of the direct measurements of the lift aerodynamic admittance are presented in Figures 4 and 5. Figure 4 shows the variations of the lift aerodynamic admittance for a selection of $\mathscr{L}_w/B$ ratios. The ordinate has been multiplied by the square of the lift slope to facilitate the interpretation of the results. All curves were found to be below Sears' linear theory and an important deficit of lift was found in the low reduced frequency range. Even though the deck cross-sections studied had poorer lift characteristics than a thin airfoil, they could generate, in the higher-frequency range, as much lift as Sears' linear theory predicted for the same input wind spectrum. The body-induced turbulence is probably the source of the observed larger lift.

TABLE 2
Time-averaged aerodynamic force coefficients (based on B) for the medium spire case, deck without railings

B/D	C_z	C_m	C'_z	C'_m
5	−0.154	0.026	4.04	1.03
10	−0.118	0.010	4.62	1.18
12.67	−0.128	−0.004	4.75	1.14

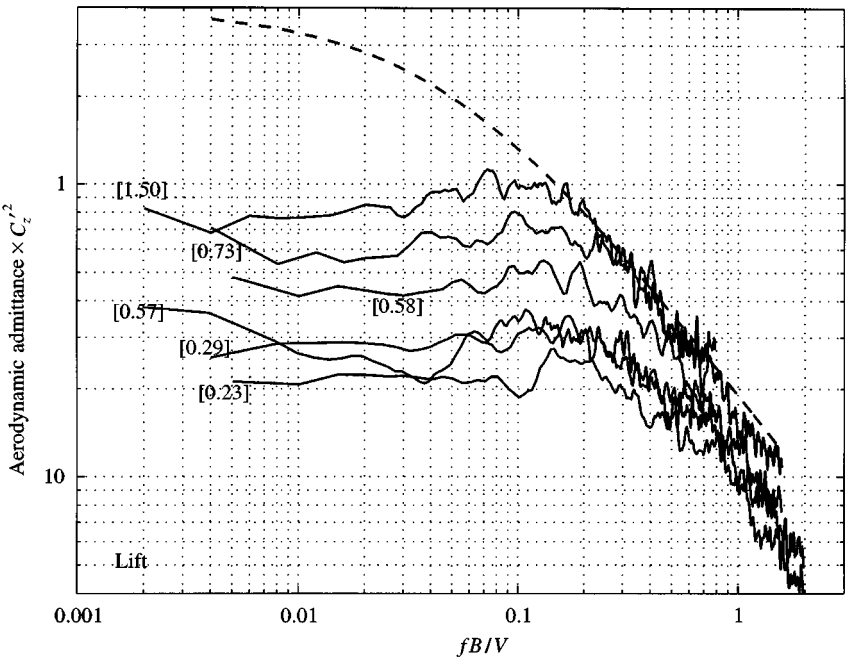

Figure 4. Lift aerodynamic admittance functions for six different $\mathscr{L}_w/B$ ratio (numbers in square brackets). The admittance has been multiplied by $C_z'^2$ to be compared with Liepmann's approximation to Sears' function for a flat plate with a lift slope of 2π (dashed line).

In Figure 5, the admittance curves are given for a constant B while the turbulent wind fields (and $\mathscr{L}_w$) are varied. It can be observed that the larger the chord-to-depth ratio or the smaller the gusts, the closer are the curves to the linear theory for a thin airfoil (dashed lines on the graphs). This was expected since the linear theory is for fully attached flow and the larger the chord-to-depth ratio, the smaller the separation region in relation to the deck width, approaching fully attached conditions. Also, the smaller the gusts, the smaller is the length of the separation bubble which favours reattachment of the flow.

3.1.3. *Measured span-wise co-coherence of the forces*

The experimentally determined span-wise distributions of the lift forces are presented here in the form of co-coherence functions or normalized co-spectra. Co-coherence is the real

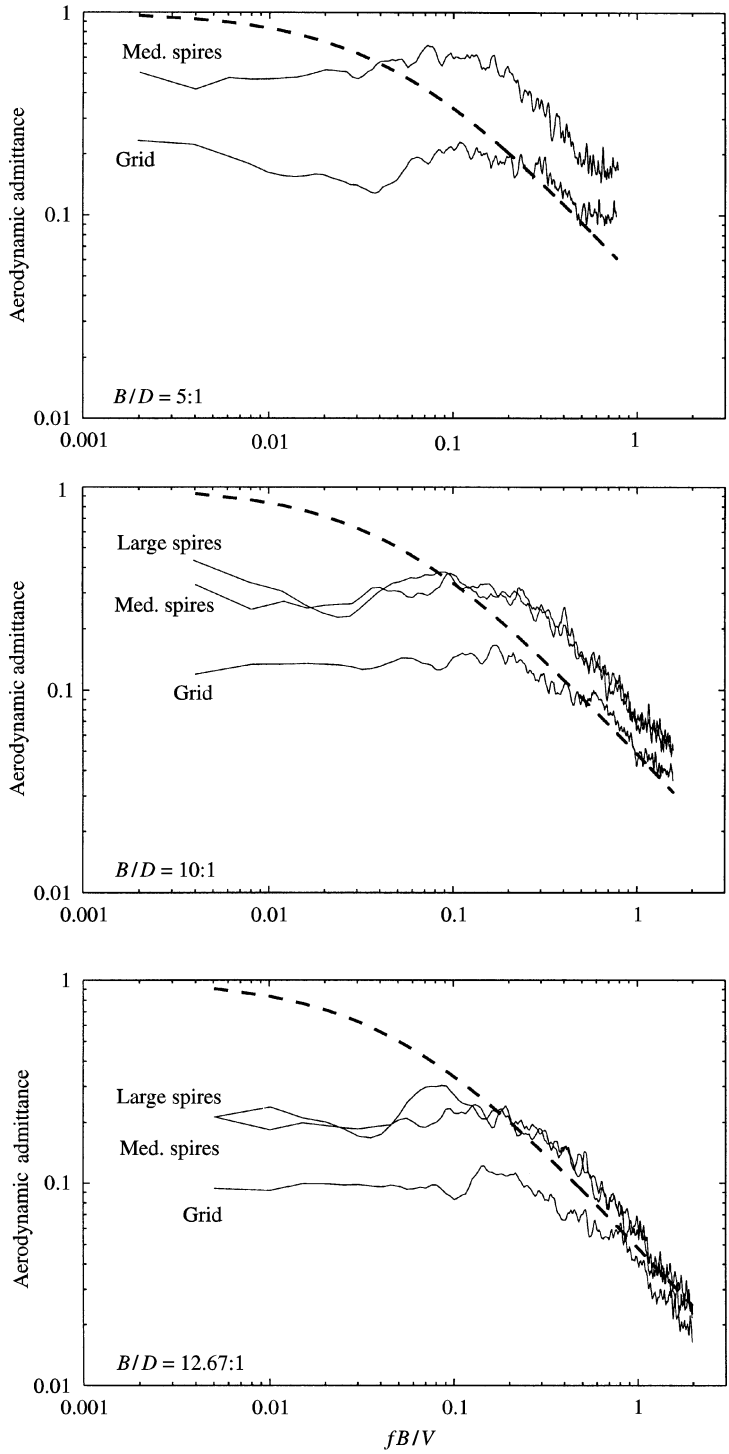

Figure 5. Variations of the lift aerodynamic admittance with reduced frequency for all cases and all B/D. The dashed line is Liepmann's approximation (13) to Sears' function.

part of the cross-spectrum of the forces between two strips normalized by the one-point spectrum. The advantage of the co-coherence presentation over the root coherence is that it can show if the forces become negatively correlated for higher frequencies or larger separations.

The span-wise co-coherence of the lift forces are presented in Figures 6 and 7. The test conditions selected are for the medium spire case and for $B/D = 5$ and 10, respectively. Also shown on the plots are the variations of the co-coherence of the w component of the wind for the medium spire case. The curves shown (solid line) are based on a fit of the measured co-coherence data with the analytical expression of the co-coherence given in Mann *et al.* (1991) based on the von Kármán spectral tensor for isotropic turbulence. The co-coherence of the forces was found to be larger than the co-coherence of the incident wind.

3.2. Applications of the 3-D Analytical Model

The two-wavenumber spectra $S_w(k_1, k_2)$ modelling the flow fields of the experiments was calculated using the von Kármán isotropic turbulence tensor (Mann 1994) and the fitted length scales given in Table 1.

Calculations of $|A(k_1)|$ and $\mathrm{coh}_L^{1/2}(k_1, \Delta y)$ using the 3-D model of Section 2.3 and Mugridge's approximation (18) were made for a series of $\mathscr{L}_w/B$ ratios corresponding to the experimental conditions. The results of the analytical calculations are presented in Figures 8 and 9.

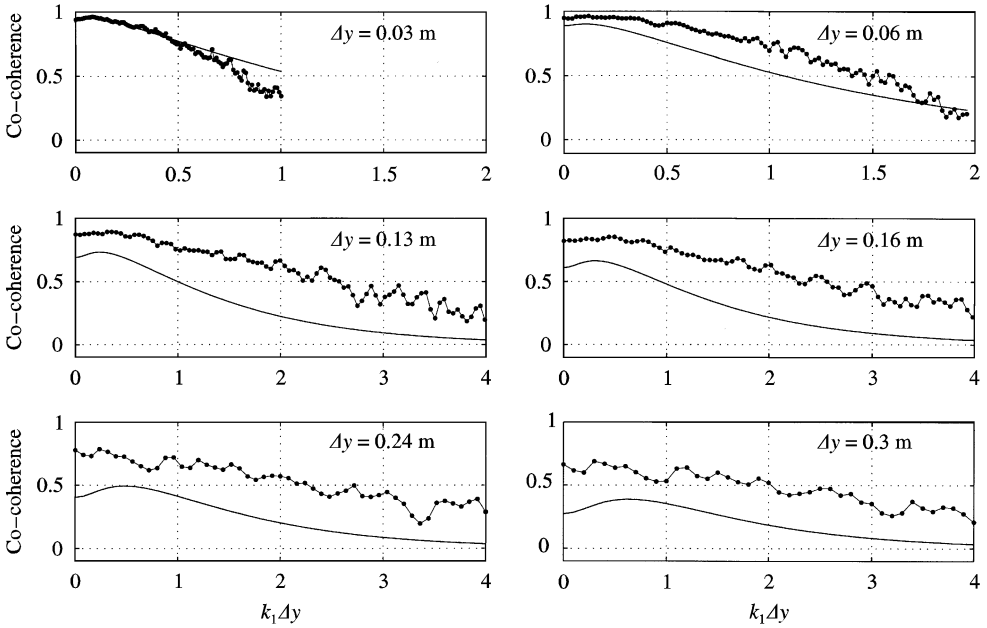

Figure 6. Variations of span-wise co-coherence as a function of $k_1\Delta y$ for the lift forces (dotted line) for $\mathscr{L}_w/B = 1.5$ compared to the wind velocity fluctuations (solid line: w with $L = 0.39$).

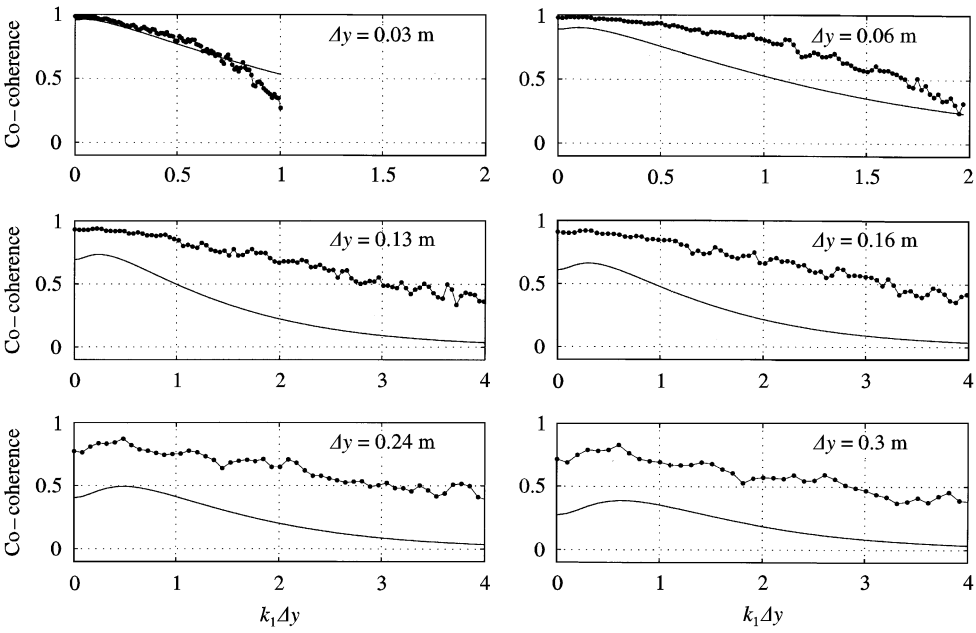

Figure 7. Variations of span-wise co-coherence as a function of $k_1\Delta y$ for the lift forces (dotted line) for $\mathscr{L}_w/B = 0.73$ compared to the wind velocity fluctuations (solid line: w with $L = 0.39$).

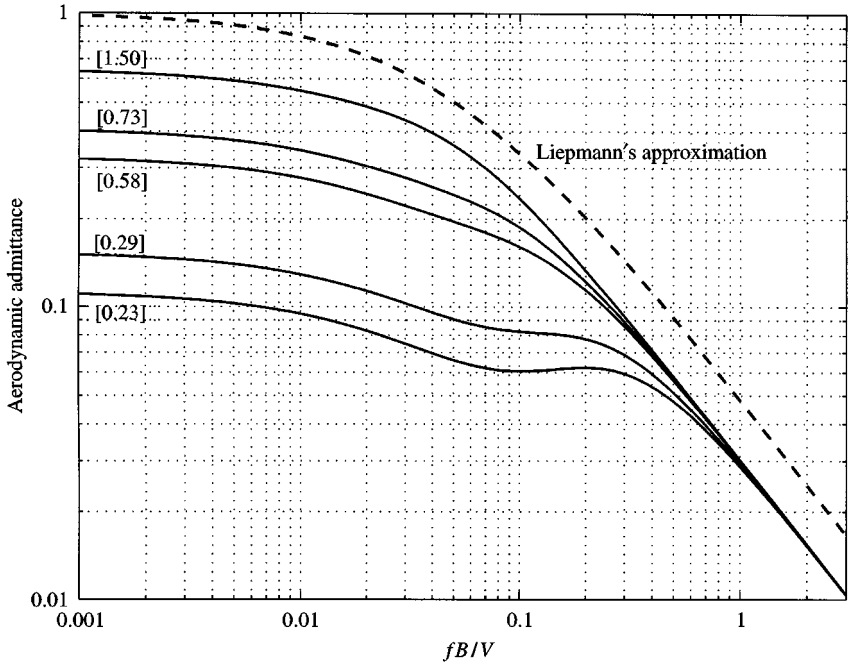

Figure 8. Analytical calculation of the aerodynamic admittance for a thin airfoil using equation (17) and Mugridge's approximation (18), for isotropic turbulence with length scale $\mathscr{L}_w$ for different values of B. The numbers in square brackets refer to the $\mathscr{L}_w/B$ ratio.

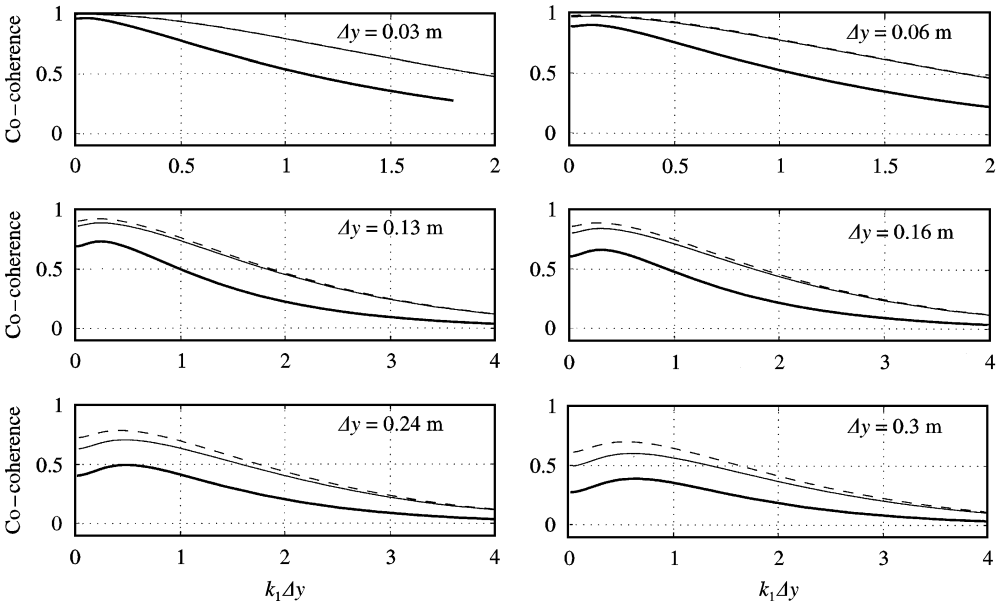

Figure 9. Analytical calculations of span-wise co-coherence of lift forces based on the 3-D model and Mugridge's approximation. Thin line: $\mathscr{L}_w/B = 1.5$; dashed line: $\mathscr{L}_w/B = 0.73$ and thick solid line: w-component of the wind fluctuations using the von Kármán spectral tensor with $L = 0.39$.

3.3. Discussion

A qualitative agreement was observed between the measured admittance and the analytically calculated admittance using the 3-D model. The agreement improves as the width-to-depth ratio increases or as the aerodynamics of the cross-sections approach the aerodynamics of a flat plate. As observed earlier (Larose 1992), the bluffer the body, the larger the admittance at higher frequencies compared to the prediction for a thin airfoil.

Another important qualitative agreement refers to an admittance value different from 1.0 for low reduced frequencies. For the larger $\mathscr{L}_w/B$ ratios, the analytical calculations did not give an admittance value larger than 0.62, even at very low reduced frequencies. Also, calculated and measured admittance curves for low $\mathscr{L}_w/B$ ratio have similar shapes. Going from low frequency to higher frequency, the curves have a trough corresponding to the largest value of S_w, then a peak corresponding to the largest value of S_L and, finally, have a sudden drop with more or less the same slope. This apparent point of inflection in the admittance curves can be observed for cases where the incident vortices are small in comparison to the deck width, resulting in a frequency shift between the peak of the wind spectrum and the peak of lift force spectrum.

Figures 10 and 11 show quantitative comparisons of the analytical calculations and direct measurements of admittance for selected $\mathscr{L}_w/B$ ratios. In Figure 10(a) it can be seen that the analytical calculation approaches the measured admittances at very low reduced frequencies. This aspect is positive since it indicates that for quasi-steady conditions, the linear 3-D theory and the experiments are in agreement. It also validates some previously published measurements of the aerodynamic admittance of bluff bodies that have been

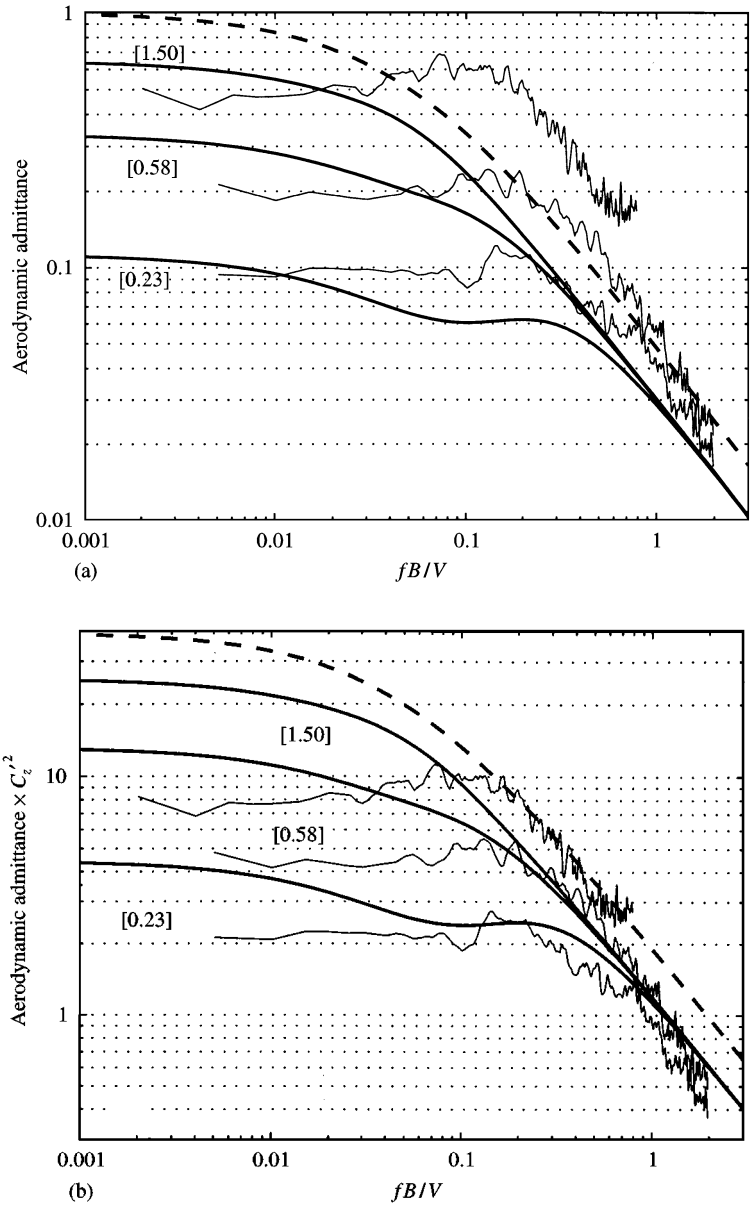

Figure 10. Comparisons between analytical calculations of lift aerodynamic admittance using the 3-D model for a thin airfoil and direct measurements on bridge decks for three $\mathscr{L}_w/B$ ratios. The dashed line is Sears' function. In (b) the ordinate has been multiplied by the square of the lift slope.

disregarded since they did not tend to 1.0 for very low reduced frequencies. For higher fB/V, the bridge decks produce body-induced turbulence that increases their admittance characteristics in comparison with the theory.

Figure 10(b) compares the product of $A_z(f)$ and $C_z'^2$ for the theory and the experiments. It indicates that if the test case approached fully reattached flow conditions, the bridge deck

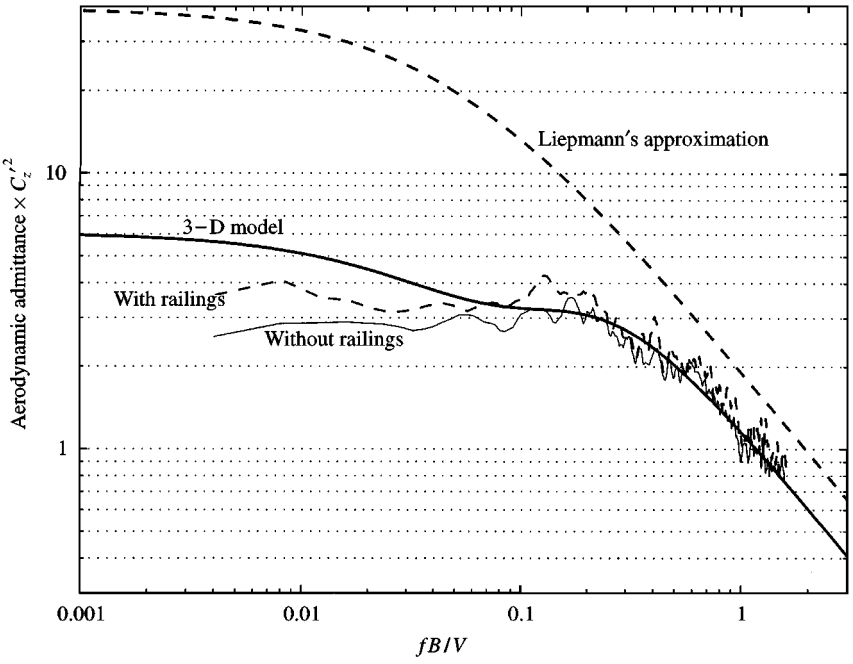

Figure 11. Comparisons between analytical calculation (thick solid line) of lift aerodynamic admittance using the 3-D model for a thin airfoil and direct measurement on a bridge deck with $B/D = 10:1$ for $\mathscr{L}_w/B = 0.29$. The ordinate has been multiplied by the square of the lift slope.

could generate similar lift to a thin airfoil. This aspect is also illustrated in Figure 11 where the case with railings, which has shown a smaller separation bubble, has lift characteristics closer to the 3-D theory than the case without railings.

3.3.1. *Span-wise co-coherence*

Qualitative agreement was also observed between analytical calculations with the 3-D model and direct measurements of the span-wise co-coherence of the forces. Most importantly $\mathrm{coh}_L^{1/2}$ was found to be larger than $\mathrm{coh}_w^{1/2}$ confirming earlier observations. The calculations also reinforced the observation reported by Larose (1997) that the lower the aerodynamic admittance the larger is the span-wise co-coherence, confirming the link between the two quantities.

Direct comparisons between calculations with the 3-D model and experiments are shown in Figure 12. The agreement is excellent for the smaller separations in the lower wave-number range. For the smallest separation, 0.03 m, the calculation overestimated the co-coherence for all $k_1\Delta y$. In fact, for this case, $\mathrm{cocoh}_L \approx \mathrm{cocoh}_w$. This observation, for very small separations in comparison to the deck width, was also reported in other studies (Larose 1992; Kimura *et al.* 1996) and cannot really be explained by the theory presented here.

It was also observed that as $\mathscr{L}_w/B$ reduces or as the influence of the small-scale turbulence increases, the 3-D model underestimated the large co-coherence measured at

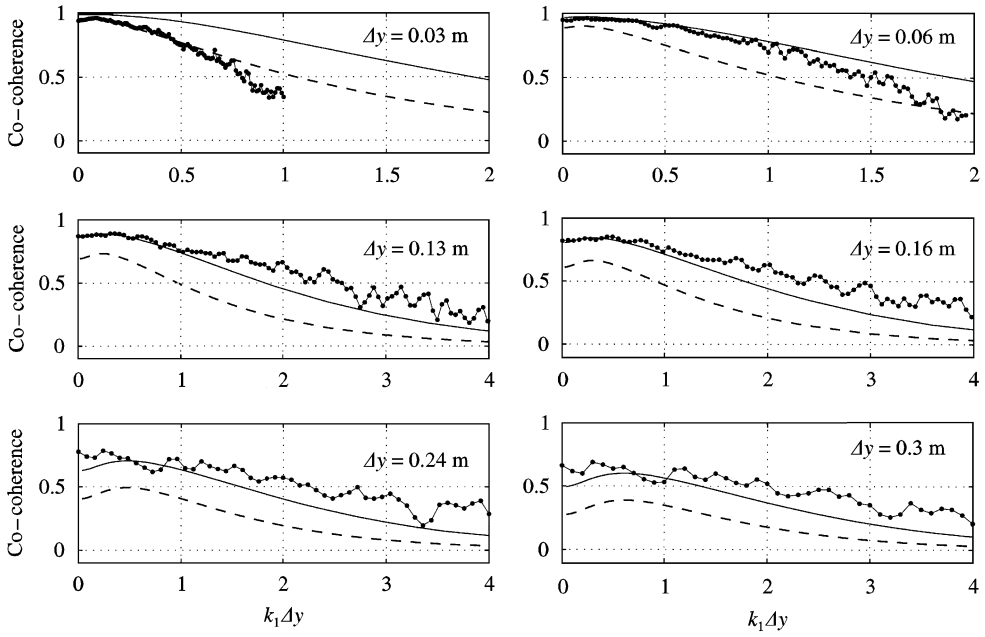

Figure 12. Comparisons between calculations (solid line) and direct measurements (dotted line) of the span-wise co-coherence of the lift forces as a function of $k_1\Delta y$ for $\mathscr{L}_w/B = 1.5$. The dashed line represents the variations of $\text{cocoh}_w^{1/2}$ of the incident wind ($L = 0.39$ m).

higher wave-numbers during the experiments. The flow mechanisms involved in the reattaching shear layer, which has shown a tendency to spread the vortices span-wise (Kiya & Sasaki 1985), can explain the difference, since the theory does not take this effect into account. This underestimation however is compensated for by a higher aerodynamic admittance obtained from the calculations when compared to the theory.

3.3.2. *Pressure distribution*

The earlier remark concerning the measurement of larger $A_z(k_1)$ than calculated for the higher frequencies for the bluffer bridge deck can partly be explained by inspection of the unsteady pressure distribution.

Figures 13 and 14 present mean and r.m.s. pressure distributions for the medium spire case for the $B/D = 5$ and 10 cases, respectively. The pressure fluctuations for the 10 : 1 case are concentrated near the leading edge, while the fluctuations for the 5 : 1 case are extended more downstream, almost to mid-chord. The latter probably represents a zone of vortices shed at or just after the reattachment point. These vortices will later mix with the wake and influence the formation of lift. It is the zone of formation of what has been called the *signature turbulence* or the body-induced turbulence.

For the 10 : 1 case, the body-induced turbulence is also produced but it is believed that it does not mix in the same manner with the wake since the convection length and velocity is greater. The vortices are likely to be distorted by the mean velocity flow field enveloping the body in accordance with the rapid distortion theory. The r.m.s. pressure distributions for

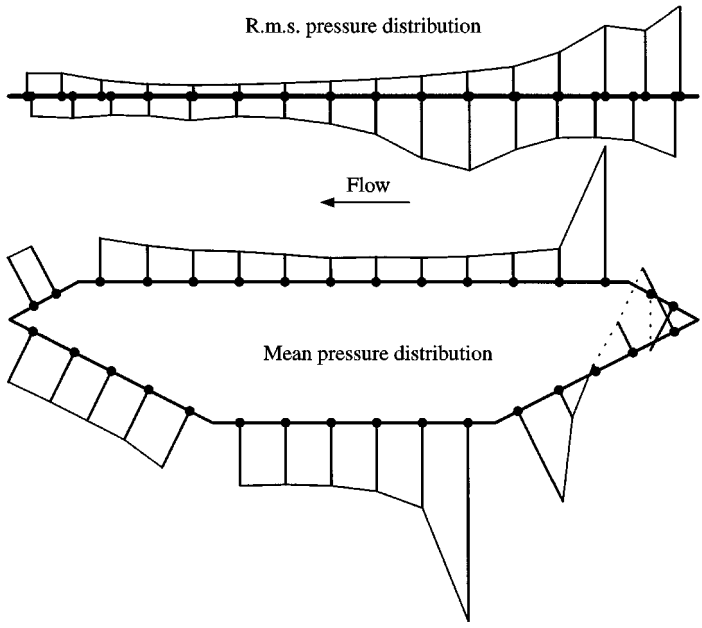

Figure 13. Surface pressure distribution on $B/D = 5$, medium spire case, without railings, 15 m s^{-1}. Scaling: depth of deck = mean C_p of 1 and r.m.s. C_p of 0.5. Polarity: negative away from the surface. The r.m.s. distribution is given for the projected tributary area.

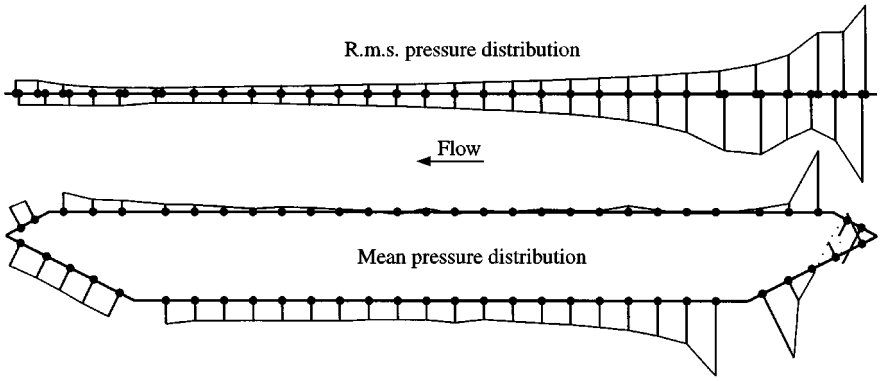

Figure 14. Surface pressure distribution on $B/D = 10$, large spire case, without railings, 15 m s^{-1}. Scaling: depth of deck = mean C_p of 1 and r.m.s. C_p of 0.5.

the 10 : 1 and 12.67 : 1 models approach the r.m.s. pressure distribution for the thin airfoil case.

4. EMPIRICAL MODEL OF THE GUST LOADING

The 3-D analytical model of the gust loading on a thin airfoil has shown qualitative agreement with the experimental description of the spatial distribution of the wind forces on

bridge decks. It has helped to understand the generation of lift on a chord-wise strip and has explained the observed larger span-wise coherence of the aerodynamic forces when compared to the span-wise coherence of the wind fluctuations.

Quantitatively, however, it has failed to reproduce closely the aerodynamic admittance of the bluffer closed-box girder bridge decks in the 0.03 to 1 reduced frequency range that is of interest for long-span bridge aerodynamics. For the more slender bridge decks, e.g. $B/D > 10$, it is believed that it could be used as an alternative to the Sears' function. In the following, an empirical model of the spatial distribution of the wind forces due to turbulence on closed-box girder bridge decks is presented. The model is inspired by the 3-D analytical model and is based on direct measurements of the gust loading.

4.1. Cross-sectional Aerodynamic Admittance

By inspection of the aerodynamic admittance curves, either obtained from analytical calculations or direct measurements, a quasi-linear dependence on the $\mathscr{L}_w/B$ ratio was depicted. This dependence is characterized by the collapse of the admittance curves shown in Figure 15, both for the analytical calculations and the experiments. The similarities between the sets of curves are remarkable. The best collapse was obtained when the ordinate was normalized by $\mathscr{L}_w/B$ to some power and when fB/V was further reduced, also by $\mathscr{L}_w/B$ to some power.

Based on this collapse, an empirical expression that could describe the aerodynamic admittance as a function of $\mathscr{L}_w/B$ and $f_r = fB/V$ was sought. The best fit of the measured aerodynamic admittance curves was obtained with the following expression:

$$\left| A_{z,m}\left(f_r, \frac{\mathscr{L}_w}{B}\right)\right|^2 = \frac{a(1+\sqrt{f_r})}{1+bf_r^2}, \tag{22}$$

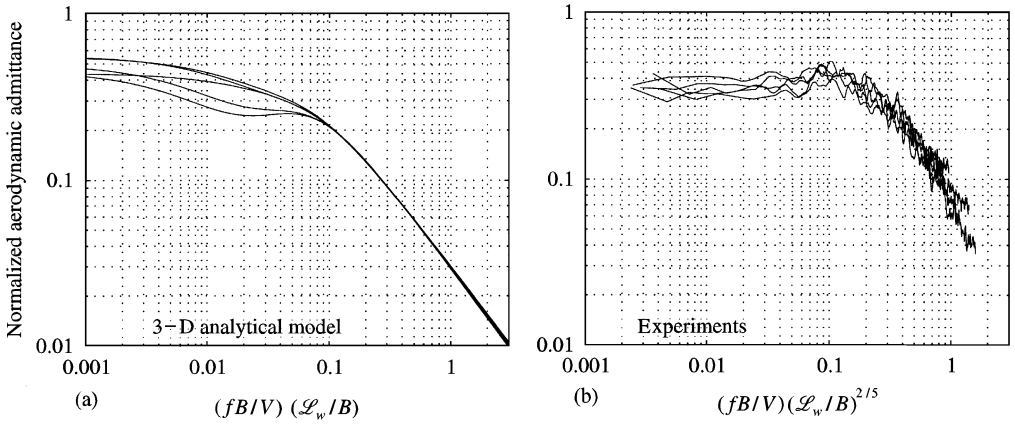

Figure 15. Collapse of lift aerodynamic admittance functions for $\mathscr{L}_w/B$ ratios varying from 1.5 to 0.23. In (a) the admittances calculated using the 3-D model have been normalized by $(\mathscr{L}_w/B)^{0{\cdot}95}$ and are plotted versus $(fB/V)/(\mathscr{L}_w/B)$. In (b) the measured admittances have been normalized by $(\mathscr{L}_w/B)^{0{\cdot}90}$ and are plotted versus $(fB/V)/(\mathscr{L}_w/B)^{2/5}$.

where

$$a = 0.34\left[\frac{\mathscr{L}_w}{B}\right]^{0\cdot95} \quad \text{and} \quad b = 9.10\left[\frac{\mathscr{L}_w}{B}\right]^{2/3} \quad \text{for lift,} \tag{23}$$

and

$$a = 0.30\left[\frac{\mathscr{L}_w}{B}\right]^{0\cdot70} \quad \text{and} \quad b = 4.30\left[\frac{\mathscr{L}_w}{B}\right]^{1/2} \quad \text{for moment.} \tag{24}$$

The limits of validity of the empirical expression above, related to the family of closed-box girder bridge decks studied here, are

$$5 < B/D < 15 \quad \text{and} \quad 0.2 < \mathscr{L}_w/B < 2. \tag{25}$$

Examples of the fit of equation (22) to the experimental data are given in Figures 16 and 17.

4.2. Span-wise Co-coherence of the Aerodynamic Forces

4.2.1. *Integral length scales*

The width of the correlation has been represented in Larose (1997) by the integral length scales

$$L^y = \int_0^\infty R_{12}(\Delta y)\,\mathrm{d}(\Delta y), \tag{26}$$

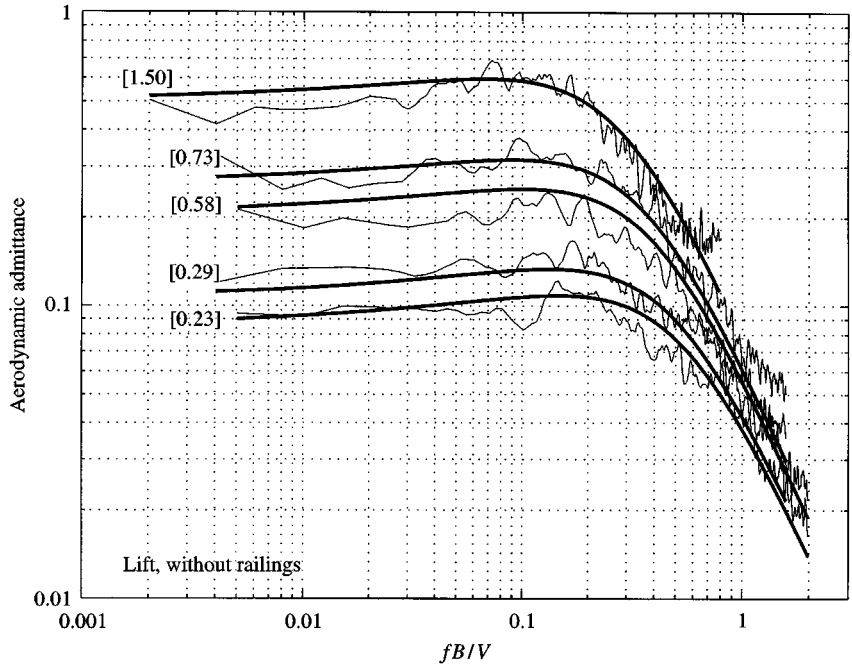

Figure 16. Variations of lift aerodynamic admittance functions for five $\mathscr{L}_w/B$ ratios (numbers in square brackets). The smooth solid lines show a fit of the measured data using equation (22).

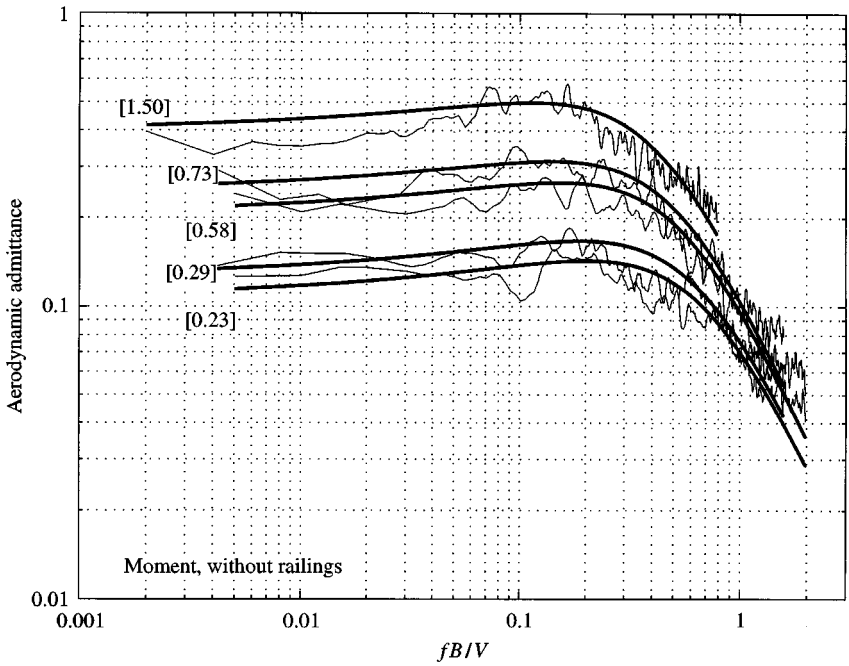

Figure 17. Variations of moment aerodynamic admittance functions for five $\mathscr{L}_w/B$ ratios (numbers in square brackets). The smooth solid lines show a fit of the measured data using equation (22).

where R_{12} is the correlation coefficient. The correlation width can be calculated from the measured correlation coefficient of the input, the w component, and directly compared to the correlation width of the output, the aerodynamic forces. On the basis of the strip assumption, for very large gusts compared to the size of the structure, $L^y_{L,M}$ should tend to L^y_w for a motionless structure.

The correlation width of the aerodynamic forces is compared in Figure 18 to the correlation width of the w component for all the test cases of this study. Also included in the graphs are results obtained by other researchers for similar streamlined bodies but for different experimental conditions.

The data points appear to fall well on one line when plotted as a function of $\mathscr{L}_w/B$ and tend towards unity as $\mathscr{L}_w/B$ increases as assumed by the strip theory. From Figure 18, the width of influence of the gusts can be determined for a given $\mathscr{L}_w/B$ ratio. For conditions representative of full-scale conditions for closed-box girder bridge decks ($1 < \mathscr{L}_w/B < 2$), the width of the influence of the vertical gusts on the lift forces was found to be at least twice the integral length scale of the gusts themselves.

4.2.2. *Force co-coherence*

By inspection of the variations of the co-coherence of the lift forces with $k_1\Delta y$ it was observed that:

(i) the shape and magnitude of the curves have more affinity with the co-coherence of v than w; this affinity is thought to be only coincidental;

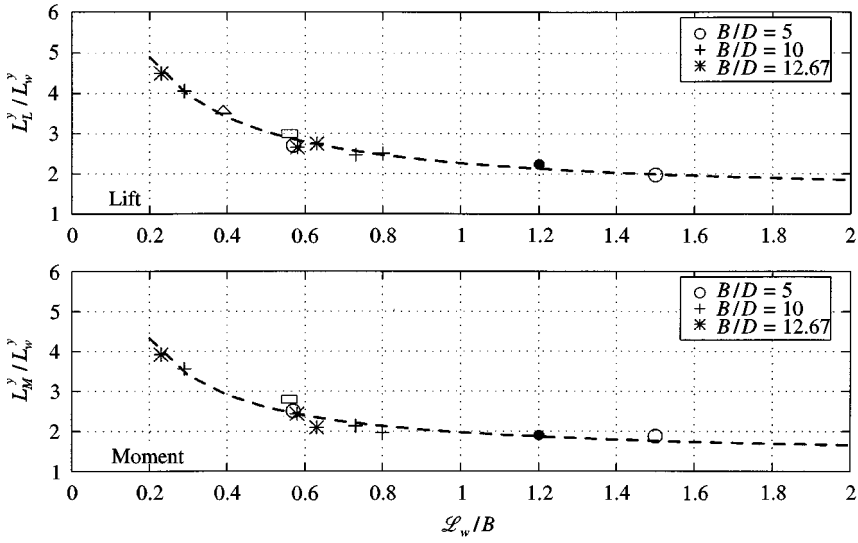

Figure 18. Variations of the ratio of the integral length scales of the forces to the integral length scales of w, $L_{L,M}^y / L_w^y$, as a function of the $\mathscr{L}_w/B$ ratio. All data points are from the present research, with the exception of: Δ, Nettleton [in Ektin (1971)]; ●, Larose (1992); □, Bogunovic Jacobsen (1995).

(ii) the decay of the force co-coherence is slower than the incident wind co-coherence and appears to be a function of the span-wise separation.

Based on these observations, an empirical expression was developed to fit the force co-coherence data (Larose 1997). It was built around the analytical expression of the co-coherence of the v component of the wind derived from the von Kármán spectrum in Mann *et al.* (1991), where the wavenumber k_1 was raised to an exponent a. This approach is similar to the approach reported by Kimura *et al.* (1996) for force co-coherence measurements on flat cylinders. The empirical expression used here to fit the data was of the form:

$$\mathrm{cocoh}_L(\eta) = \frac{2}{\Gamma(\frac{5}{6})}\left(\frac{\eta}{2}\right)^{5/6}\left[\mathrm{K}_{5/6}(\eta) + \frac{3(\Delta y k_1^a)^2}{3\eta^2 + 5(\Delta y k_1^a)^2}\,\eta \mathrm{K}_{1/6}(\eta)\right], \tag{27}$$

where

$$\eta = k_1^a \Delta y \sqrt{1 + \frac{1}{(k_1^a L_L)^2}}, \tag{28}$$

and $\mathrm{K}_{1/6}$ and $\mathrm{K}_{5/6}$ are modified Bessel functions of the second kind. The exponent a and the length scale L_L were kept as floating parameters for the least-squares fits.

At first the calculated force co-coherence curves using the 3-D model and Mugridge's approximation were fitted with equation (27). The results of the fits for three $\mathscr{L}_w/B$ ratios are shown in Figure 19.

The best fit was obtained when $a = 0.95$ and when L_L, the length scale related to the lift forces, was varied as a function of Δy, as seen in Figure 19. It was also observed that if L_L

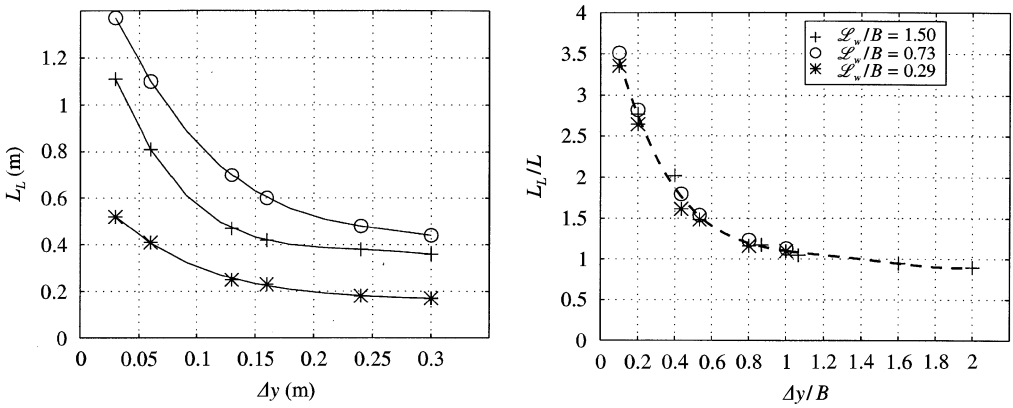

Figure 19. Results of the fit of the co-coherence of the lift forces calculated using the 3-D model and Mugridge's approximation and fitted with equation (27) with k_1^a, where $a = 0.95$.

was normalized by L, the von Kármán length scale describing the input wind field, and plotted versus normalized separation $\Delta y/B$, the results fitted well on one line and tended to a value slightly lower than 1 (see the right-hand-side graph of Figure 19).

In a similar fashion, all measured co-coherence of the aerodynamic forces of this study were fitted with equation (27) with k_1^a, keeping the exponent a and the length scale L_L as floating parameters for the least-squares fits. The results for all $\mathscr{L}_w/B$ ratios are shown in Figure 20. It can be observed from Figure 20 that the normalized lift length scale L_L/L also tends to a value near 1 for larger $\Delta y/B$ and that the curves are grouped by chord-to-depth ratio, B/D. For example, the $\mathscr{L}_w/B = 1.5$ and 0.57 are from $B/D = 5$ in two different cases, and showed exactly the same L_L/L and a for both cases.

For separations smaller than half the deck width it is clear that the larger the deck width, the larger are the lift length scales. It indicates that the longer the incident large eddies are being distorted over the deck, the larger is the possibility of forming secondary cross-flow, and the larger the span-wise coherence.

The exponents a also appeared to be grouped by B/D ratios; the larger the deck width, the smaller the exponent up to a certain plateau. This exponent gives an indication of the rate of decay of the co-coherence with frequency. Bluff bodies have a tendency to spread the separated flow vortices (body-induced turbulence) span-wise (Kiya & Sasaki 1985) as they are convected over the body. Since the larger the after-body, the larger this effect, this could explain the observed relatively larger influence of the higher frequency gusts for the wider decks, represented by smaller exponents a.

The value of a for $B/D = 10$ and 12.67 appeared to tend towards 0.75 for larger $\Delta y/B$. This is in agreement with results by Kimura *et al.* (1996), who obtained $a = 0.74$ for flat cylinders with $B/D = 8.7$.

It was observed that, at high frequencies, the measured co-coherence were in most cases larger than that predicted by the analytical model (see Figure 12). The failure of the 3-D analytical model (chain-dotted line in Figure 20 and solid lines on Figure 12) has probably to do with separated flow vortices, which may have strong span-wise co-coherence. Separated flow is out of reach of the analytical model.

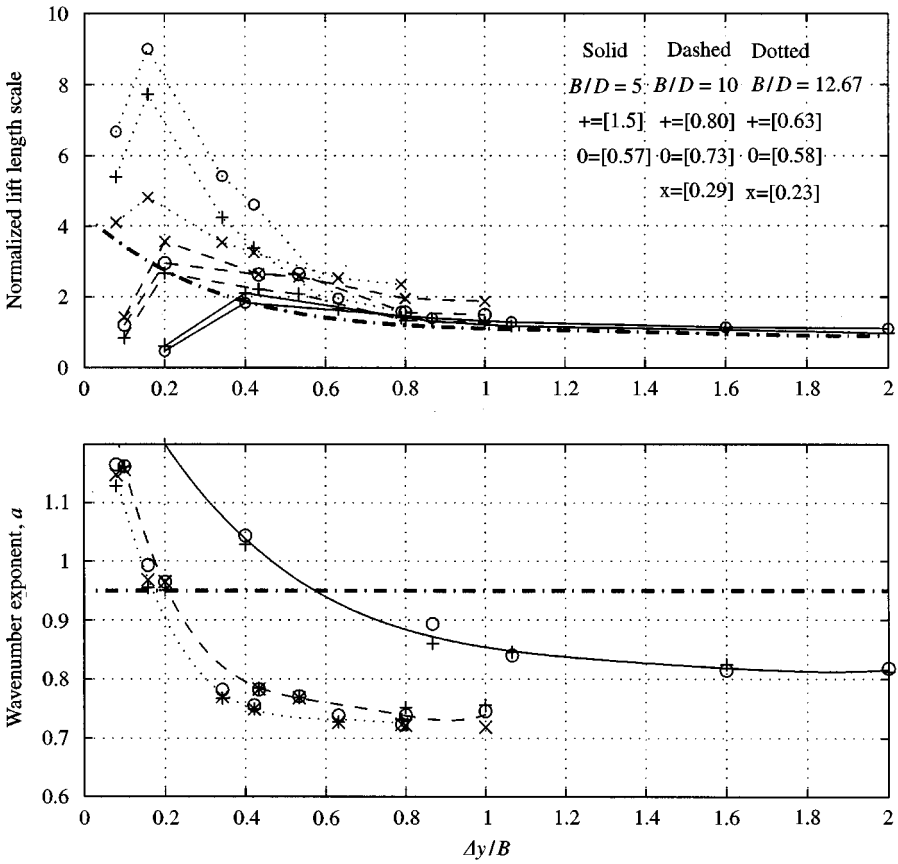

Figure 20. Results of the fit of the measured co-coherence of the lift forces as a function of $\Delta y/B$. The ordinate of the top graph is the lift length scale L_L obtained from the fit of equation (27) and normalized by the length scale L of the incident flow. The chain-dotted line refers to the theoretical calculations with the 3-D model. The wavenumber exponent refers to a in k_1^a.

4.2.3. *Empirical formulations*

Relationships between L_L, a and $\Delta y/B$ were extracted from the results presented above. In combination with the analytical description of the incident wind field, they form the basis of an empirical model of the spatial distribution of the aerodynamic forces on closed-box girder bridge decks of the cross-section family studied here.

The span-wise co-coherence of the lift forces can be expressed as a function of $\Delta y, k_1, \mathscr{L}_w/B, B/\mathrm{D}$ by equation (27), where

$$\eta = k_1^a \Delta y \sqrt{1 + \frac{1}{(k_1^a L_L)^2}}, \tag{29}$$

$$a = \left(\frac{B}{D}\right)^4 \frac{(p + \frac{\Delta y}{B})^2}{(q + r\frac{\Delta y}{B})^2}, \quad p = 0.16, \quad q = 0.0788, \quad r = 0.935, \tag{30}$$

$$L_L = L \frac{(p + \frac{\Delta y}{B})^2}{(q + r\frac{\Delta y}{B})^2}, \quad p = 1.0, \quad q = 0.46, \quad r = 1.42. \tag{31}$$

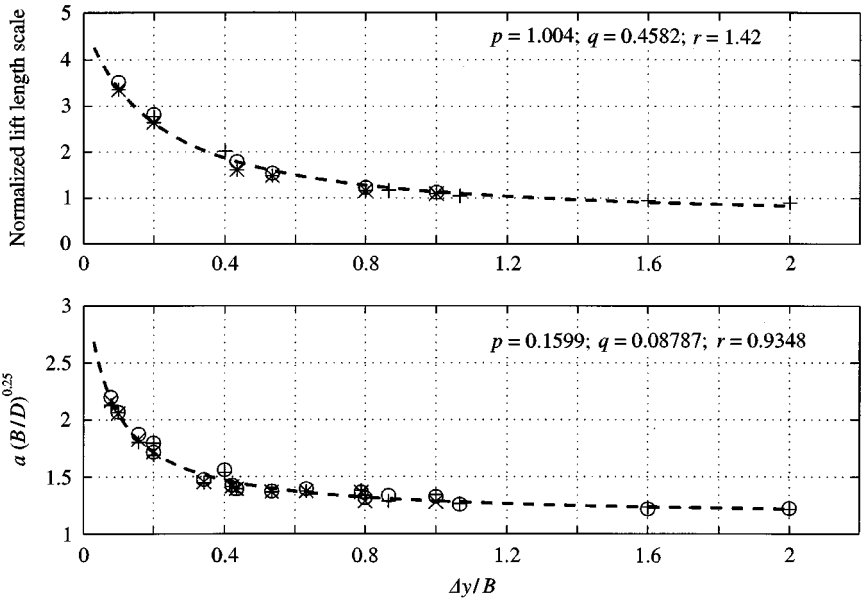

Figure 21. Collapse of L_L and a based on the fit of the co-coherence of the lift forces with equation (27) with k_1^a for all cases.

A graph showing the variations of L_L and a as a function of $\Delta y/B$ for the lift forces is given in Figure 21. For the sake of simplicity, the variations of L_L/L with Δy extracted from the calculations of co-coherence with the 3-D model were used to represent L_L in equation (31). The effect of this simplification for the evaluation of the gust loading on a large bridge span was found to be negligible (Larose 1997) since the calculations are normally made for $\Delta y/B$ up to between 50 and 70.

4.2.4. *Co-coherence of the overturning moment*

The analysis described above was repeated for the aerodynamic overtuning moment of the bridge decks. Similar variations of the L_M/L and a with $\Delta y/B$ were obtained when compared with the lift force results. The scatter of L_M/L for $\Delta y/B < 0.50$ was lower than observed for the lift forces and coincidently followed the variations of L_L extracted from the 3-D analytical model. The exponent a was found to be slightly higher than that for the lift indicating a slightly more rapid decay of the moment co-coherence. The best fit of the exponent a was obtained with

$$a = \left(\frac{B}{D}\right)^{1/0{\cdot}15} \frac{\left(p + \frac{\Delta y}{B}\right)^2}{\left(q + r\frac{\Delta y}{B}\right)^2}, \quad p = 0.098, \quad q = 0.059, \quad r = 0.970, \tag{32}$$

as shown in Figure 22.

5. CONCLUSIONS

An analytical model that departs from the strip assumption was presented to describe the gust loading on a thin airfoil in isotropic turbulence. The 3-D model is based on a two

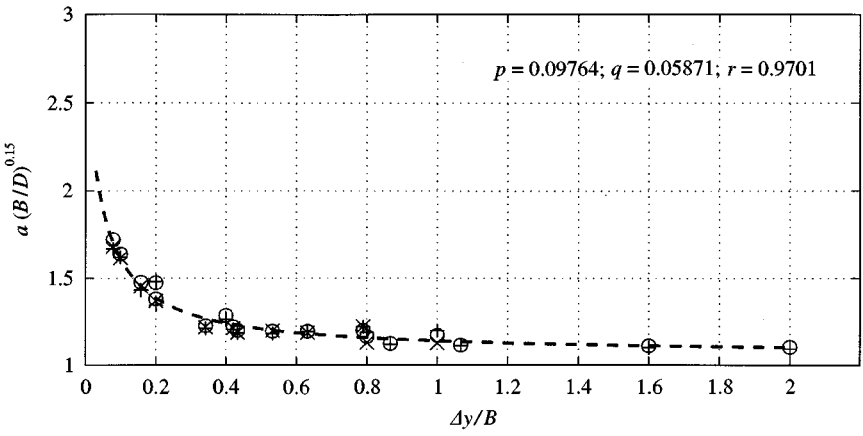

Figure 22. Collapse of a based on the fit of the co-coherence of the overturning moment with equation (27) with k_1^a for all cases.

arbitrary horizontal wavevector analysis as opposed to the fully correlated sinusoidal gust analysis due to Sears.

The 3-D model has shown qualitative agreement with the experimental description of the aerodynamic admittance and the spatial distribution of the gust loading on bridge decks. It has helped understand the generation of lift on a chord-wise strip and has explained the observed larger span-wise co-coherence of the forces when compared to the co-coherence of the incident wind.

Quantitatively, however, the 3-D analytical model did not reproduce adequately some aspects of the gust loading on the bluffer closed-box girder bridge decks. An empirical model was thus derived to describe the gust loading on the family of closed-box girder bridge decks of this study. The empirical model departs from the strip assumption and was inspired by the analytical description of the incident wind field as well as the 3-D model of the spatial distribution of the aerodynamic forces.

It is likely that the empirical model could be extended to the cross-sections of other closed-box girder bridge decks, provided that the aerodynamic characteristics approached the flat-plate characteristics. For relatively open truss-girder bridge decks, the strip assumption would certainly provide a fair approximation at low frequencies, but the body-induced turbulence will dominate at high frequencies. In this situation, the recommendation is to rely on *ad hoc* wind tunnel tests to determine the gust loading.

ACKNOWLEDGEMENTS

The financial support of the COWI foundation for the experimental part of this research is gratefully acknowledged, as well as the research scholarship provided by the Danish Research Academy and the Danish Maritime Institute.

REFERENCES

BLAKE, W. K. 1986 *Mechanics of Flow-Induced Sound and Vibration*, Vol. 1. Orlando, FL: Academic Press, p. 743.

Bogunovic Jakobsen, J. 1995 Fluctuating wind load and response of a line-like engineering structure with emphasis on motion-induced wind forces. Ph.D. Thesis, The Norwegian Institute of Technology, Trondheim, Norway.

Davenport, A. G. 1962 The response of slender, line-like structures to a gusty wind. *Proceedings of Institution of Civil Engineers* **23,** 389–408.

Ektin, B. 1971 *Dynamic of Atmospheric Flight*, pp. 547–548. New York: Wiley.

Fung, Y. C. 1969 *An Introduction to the Theory of Aeroelasticity*, New York: Dover Publications Inc.

Graham, J. M. R. 1970 Lifting-surface theory for the problem of an arbitrary yawed sinusoidal gust incident on a thin aerofoil in incompressible flow. *Aeronautical Quarterly*, **21,** 182–198.

Jackson, R., Graham, J. M. R. & Maull, D. J. 1973 The lift on a wing in a turbulent flow. *Aeronautical Quarterly* **24,** 155–166.

Kimura, K., Fujino, Y., Nakato, S. & Tamura, H. 1996 Characteristics of the buffeting forces on flat cylinders. *Proceedings of 3rd International Colloquium on Bluff Body Aerodynamics and Applications*, Blacksburg, Virginia, USA, July.

Kiya, M. & Sasaki, K. 1985 Structure of large-scale vortices and unsteady reverse flow in the reattaching zone of a turbulent separation bubble. *Journal of Fluid Mechanics* **154**, 463–491.

Larose, G. L. 1992 The response of a suspension bridge deck to turbulent wind: the taut strip model approach. M.E.Sc. Thesis, University of Western Ontario, Canada.

Larose, G. L. 1997 The dynamic action of gusty winds on long-span bridges. Ph.D. Thesis, Technical University of Denmark, Lyngby, Denmark.

Larose, G. L., Davenport, A. G. & King, J. P. C. 1993 On the unsteady aerodynamics forces acting on a bridge deck in turbulent flow. *Proceedings of the 7th US National Conference on Wind Engineering*, U.C.L.A. Los Angeles, USA, June, pp. 373–382.

Liepmann, H. W. 1952 On the application of statistical concepts to the buffeting problem. *Journal of the Aeronautical Sciences* **19,** 793–800.

Mann, J. 1994 The spatial structure of neutral atmospheric surface-layer turbulence. *Journal of Fluid Mechanics* **273,** 141–168.

Mann, J. 1995 The strip assumption in bridge aerodynamics. Unpublished Technical Note, Danish Maritime Institute.

Mann, J., Kristensen, L. & Courtney, M. S. 1991 The Great Belt Coherence Experiment—A study of atmospheric turbulence over water. Risø Report No. R-596.

Melbourne, W. H. 1982 Comparison of model and full-scale tests of a bridge and chimney stack. *Proceedings of International Workshop on Wind Tunnel Modelling*, Maryland, USA, pp. 637–653.

Mugridge, B. D. 1971 Gust loading on a thin aerofoil. *Aeronautical Quarterly* **22,** 301–310.

Sankaran, R. & Jancauskas, E. D. 1993 Measurements of cross-correlation in sparated flows around bluff cylinders. *Journal of Wind Engineering and Industrial Aerodynamics* **49,** 279–288.

Vickery, B. J. 1966 Fluctuating lift and drag of a long cylinder of square cross-section in a smooth and turbulent stream. *Journal of Fluid Mechanics* **25,** 481–494.